

## Quenched Disordered Ferromagnets\*

---

### Wolfhard Janke<sup>†</sup>

*Institut für Theoretische Physik, Universität Leipzig,  
Augustusplatz 10/11, D-04109 Leipzig, Germany  
E-mail: wolfhard.janke@itp.uni-leipzig.de*

### Bertrand Berche and Christophe Chatelain

*Laboratoire de Physique des Matériaux, UMR CNRS 7556, Université Henri Poincaré,  
Nancy 1, F-54506 Vandœuvre les Nancy Cedex, France  
E-mail: {berche, chatelai}@lpm.u-nancy.fr*

### Pierre-Emmanuel Berche

*Groupe de Physique des Matériaux, UMR CNRS 6634, Université de Rouen,  
F-76801 Saint Etienne du Rouvray Cedex, France  
E-mail: pierre.berche@univ-rouen.fr*

### Meik Hellmund

*Institut für Mathematik, Universität Leipzig,  
Augustusplatz 10/11, D-04109 Leipzig, Germany  
E-mail: meik.hellmund@math.uni-leipzig.de*

We review and compare different approaches for studying the influence of quenched, random disorder in three-dimensional Ising and Potts models for ferromagnets subject to impurities. From a theoretical view point, field theoretic renormalization group studies provide quite accurate results. Experiments carried out on crystalline mixtures of compounds lead to measurements of critical exponents as accurate as three digits. Numerically, extensive Monte Carlo simulations are shown to be of comparable accuracy. Finally, we also discuss recently generated high-temperature series expansions for the free energy and susceptibility. Within this approach, using the star-graph expansion technique, quenched disorder averages can be calculated exactly while keeping the disorder strength  $p$  as well as the dimension  $d$  as symbolic parameters.

*XXIIIrd International Symposium on Lattice Field Theory  
25-30 July 2005  
Trinity College, Dublin, Ireland*

---

\*Work partially supported by DFG grant No. JA 483/17-3. We gratefully acknowledge the computer-time grants hlz061 of NIC, Jülich, h0611 of LRZ, München, 062 0011 of CINES, Montpellier, and 2000007 of CRIHAN, Rouen.

<sup>†</sup>Speaker.

## 1. Introduction

Since many years random Ising and Potts models have served as paradigmatic systems in which the influence of quenched disorder may be studied through different techniques. Here we describe four of them: The renormalization group (RG) approach, experimental measurements, Monte Carlo simulation and high-temperature series expansions.

Pure Potts models show either first- or second-order phase transitions, depending on the dimension  $d$  and the number of states  $q$ . Since in the second-order case the specific-heat exponent  $\alpha$  is non-negative for this class of models, the Harris criterion [1] suggests for the corresponding disordered systems either the appearance of a new random fixed point ( $d = 2$ ,  $q = 3, 4$  and  $d = 3$ ,  $q = 2$ ) or logarithmic corrections to the pure fixed point ( $d = 2$ ,  $q = 2$ ). At first-order phase transitions, randomness softens the transitions [2]. For  $d = 2$  even infinitesimal disorder induces a continuous transition [3, 4, 5, 6], whereas for  $d = 3$ ,  $q > 2$  a tricritical point at a finite disorder strength is expected [5].

For the three-dimensional (3D) disordered Ising model, RG calculations were considered quite early [1, 7] and since then many groups performed very skillful RG calculations (for recent reviews, see Refs. [8, 9]). On the experimental side, measurements on crystalline mixtures of difluoride of different transition metals, e.g., magnetic  $\text{FeF}_2$  substituted with non-magnetic  $\text{ZnF}_2$ , were performed in the same period over two decades, gaining in refinement and accuracy (see early results of Birgeneau *et al.* in Ref. [10], for a review see, e.g., Ref. [11]). For the third aspect of simulations, technical progress made by computer manufacturers enabled more and more accurate simulations (which started for disordered systems in 3D, e.g., with Landau in Ref. [12]) and the study of disordered magnetic systems benefited from the development of parallel computing. Monte Carlo simulators thus competed in performance (for a review, see, e.g., Ref. [8]). The fourth approach consists of generating high-temperature series expansions and their analyses. While conceptually quite straightforward and therefore also considered very early, it is technically rather demanding as we shall see below.

In the major part of this paper we will first give in Sect. 2 a review of some recent progress in studies of the 3D disordered Ising model, emphasising the role of universality and its difficult emergence when trying to reconcile theoretical, experimental, and computational predictions. Several reviews are available, e.g. Refs. [8], [9] or [13], so we will not attempt for exhaustive citations to previous works. Section 3 is devoted to a discussion of recent Monte Carlo simulations and high-temperature series expansions of the 3D 4-state Potts model. Our conclusions are presented in Sect. 4.

## 2. Disordered Ising model

### 2.1 RG calculation of critical exponents

Long distance properties of the Ising model near its second-order phase transition are described in field theory by an effective Ginzburg-Landau-Wilson Hamiltonian

$$H_{\text{Ising}}[\varphi] = \int d^d \mathbf{r} \left[ \frac{1}{2} (\nabla \varphi(\mathbf{r}))^2 + \frac{1}{2} m_0^2 \varphi^2(\mathbf{r}) + \frac{\tilde{u}_0}{4!} \varphi^4(\mathbf{r}) \right], \quad (2.1)$$

where  $m_0^2$  is the bare coupling proportional to the deviation  $T - T_c$  from the critical point and  $\varphi(\mathbf{r})$  is a bare scalar field. Quenched randomness enters in this formulation through a random temperature-like variable  $\Delta$  added to  $m_0^2$ ,

$$H[\varphi, \Delta] = \int d^d \mathbf{r} \left[ \frac{1}{2} (\nabla \varphi(\mathbf{r}))^2 + \frac{1}{2} (m_0^2 + \Delta(\mathbf{r})) \varphi^2(\mathbf{r}) + \frac{\tilde{u}_0}{4!} \varphi^4(\mathbf{r}) \right], \quad (2.2)$$

where  $\Delta(\mathbf{r})$  is drawn from, e.g., a Gaussian probability distribution of zero mean and dispersion  $\sigma^2$ ,  $\mathcal{P}(\Delta) = (2\pi\sigma^2)^{-1} \exp(-\Delta^2/2\sigma^2)$ . For a specific disorder realization  $[\Delta]$ , the partition function and the free energy read as usually  $Z[\Delta] = \int \mathcal{D}[\varphi] e^{-\beta H[\varphi, \Delta]}$  and  $F[\Delta] = -\beta^{-1} \ln Z[\Delta]$ . The average over the quenched disorder distribution  $\mathcal{P}(\Delta)$  then requires to calculate quantities like  $[F[\Delta]]_{\text{av}} = -\beta^{-1} \int \mathcal{D}[\Delta] \ln Z[\Delta] \mathcal{P}(\Delta)$ . This is performed through the introduction of  $n$  replicas of the model (labelled by  $\alpha$ ). Averaging over quenched disorder one ends up with an effective Hamiltonian with cubic anisotropy where the replicas are coupled through a new parameter  $v_0$

$$H_{\text{replicas}}[\varphi] = \int d^d \mathbf{r} \left[ \frac{1}{2} \sum_{\alpha=1}^n [(\nabla \varphi_\alpha(\mathbf{r}))^2 + m_0^2 \varphi_\alpha^2(\mathbf{r})] + \frac{u_0}{4!} \sum_{\alpha=1}^n \varphi_\alpha^4(\mathbf{r}) + \frac{v_0}{4!} \left( \sum_{\alpha=1}^n \varphi_\alpha^2(\mathbf{r}) \right)^2 \right]. \quad (2.3)$$

Here the bare coupling  $u_0$ , proportional to  $\tilde{u}_0$ , is positive and the bare coupling  $v_0$ , proportional to  $-\sigma^2$ , is negative. To the  $n$ -component Hamiltonian (2.3) the usual (but rather elaborate) RG machinery can be applied. The properties of the random Ising model are eventually obtained when taking the limit  $n \rightarrow 0$ ,  $\ln Z = \lim_{n \rightarrow 0} (Z^n - 1)/n$ .

Under a change of length scale by a factor  $\mu$ , the field and couplings are renormalised according to

$$\varphi = Z_\phi^{1/2} \phi, \quad m_0^2 = Z_{m^2} m^2, \quad u_0 = \mu^\varepsilon \frac{Z_u}{Z_\phi^2} u, \quad v_0 = \mu^\varepsilon \frac{Z_v}{Z_\phi^2} v, \quad (2.4)$$

where  $\varepsilon = 4 - d$ . The RG functions are defined by differentiation at fixed bare parameters,

$$\beta_u(u, v) = \left. \frac{\partial u}{\partial \ln \mu} \right|_0, \quad \beta_v(u, v) = \left. \frac{\partial v}{\partial \ln \mu} \right|_0, \quad (2.5)$$

$$\gamma_\phi(u, v) = \left. \frac{\partial \ln Z_\phi}{\partial \ln \mu} \right|_0, \quad \gamma_{m^2}(u, v) = \left. \frac{\partial \ln Z_{m^2}}{\partial \ln \mu} \right|_0. \quad (2.6)$$

The theoretical challenge is the perturbative computation of these functions [14, 15] (they are known up to 6 loops), removing divergences which occur in the asymptotic limit by controlled rearrangement of the series for the vertex functions. Eventually, given the fact that these expansions are divergent asymptotic series, reliable results can only be expected after complicated resummation procedures [16]. Fixed points are then solutions of  $\beta_u(u^*, v^*) = \beta_v(u^*, v^*) = 0$ , the stability of which is controlled by a stability matrix  $\frac{\partial \beta_i}{\partial u_j}$  with eigenvalues which besides the standard critical exponents also govern the corrections to scaling (exponent  $\omega$ ).

At that point, it is quite easy to read off the critical exponents. Consider for example the pair correlation function of bare fields  $\langle \varphi(0) \varphi(\mathbf{r}) \rangle$ . Under a change of length scale  $\mu$ , it renormalises to  $Z_\phi(\mu) \langle \phi(0) \phi(\mathbf{r}) \rangle$ . In the same manner, for another dilatation parameter,  $\mu s$ , one has  $\langle \varphi(0) \varphi(s\mathbf{r}) \rangle \rightarrow Z_\phi(\mu s) \langle \phi(0) \phi(s\mathbf{r}) \rangle$ . The ratio from this latter to the previous expression leads to

$$\frac{\langle \phi(0) \phi(s\mathbf{r}) \rangle}{\langle \phi(0) \phi(\mathbf{r}) \rangle} = \frac{Z_\phi(\mu) \langle \varphi(0) \varphi(s\mathbf{r}) \rangle}{Z_\phi(\mu s) \langle \varphi(0) \varphi(\mathbf{r}) \rangle}. \quad (2.7)$$

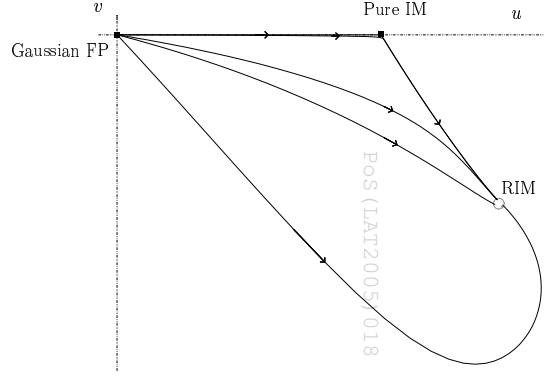


**Figure 1:** RG flows in the  $(u, v)$  plane. The points denoted “Gaussian FP”, “Pure IM” and “RIM” are respectively the Gaussian, the pure Ising model and the random Ising model fixed point.

This expression gives the algebraic decay of the two-point correlation function of renormalised fields  $\langle \phi(0)\phi(\mathbf{r}) \rangle \sim |\mathbf{r}|^{-(d-2+\eta_\phi)}$  in terms of the pair correlation function of the bare fields which are described by mean-field theory (MFT), i.e., at the Gaussian fixed point (FP),  $\langle \phi(0)\phi(\mathbf{r}) \rangle \sim |\mathbf{r}|^{-(d-2)}$  ( $\eta_{\text{MFT}} = 0$ ). The ratio  $\frac{Z_\phi(\mu)}{Z_\phi(\mu s)} = e^{\int_{\mu s}^{\mu} \gamma_\phi d \ln \mu}$  evaluated at the new FP gives  $s^{-\gamma_\phi^*}$  and leads to

$$\frac{\langle \phi(0)\phi(s\mathbf{r}) \rangle}{\langle \phi(0)\phi(\mathbf{r}) \rangle} \sim s^{-(d-2+\gamma_\phi^*)}, \quad (2.8)$$

where  $\langle \phi(0)\phi(\mathbf{r}) \rangle$  plays here the role of an amplitude and from which one reads off the value of the critical exponent at this FP:

$$\eta_\phi = \gamma_\phi^*. \quad (2.9)$$

Following the same argument, the scaling dimension  $1/\nu$  of the (renormalised) temperature field  $m^2$  is given at the random fixed point in terms of the MFT value,  $1/\nu_{\text{MFT}} = 2$ , and one gets

$$\frac{1}{\nu} = 2 - \gamma_{m^2}^*. \quad (2.10)$$

From these two exponents, the others may be deduced by scaling arguments, describing the leading singularities of the physical quantities, e.g., of the magnetic susceptibility:

$$\chi(\tau) \sim \Gamma_\pm |\tau|^{-\gamma}, \quad \gamma = \nu(2 - \eta_\phi). \quad (2.11)$$

In the non-asymptotic regime, the system approaches criticality in a more complex way and this is where corrections to scaling appear,

$$\chi(\tau) \sim \Gamma_\pm |\tau|^{-\gamma} (1 + \Gamma'_\pm |\tau|^{\nu\omega} + \Gamma''_\pm |\tau|^{2\nu\omega} + \dots), \quad (2.12)$$

where the scaling dimension  $\omega$  corresponds to the negative of the leading irrelevant RG eigenvalue,  $\omega = -|y_3|$ , as it is usually denoted, and the dots in Eq. (2.12) stand for higher-order irrelevant corrections.

Besides the critical exponents, also combinations of critical amplitudes and correction-to-scaling exponents are universal quantities. In order to describe the approach to criticality it is common practice, especially in experiments and simulations, to introduce effective exponents through

$$\chi(\tau) \sim \Gamma_\pm |\tau|^{-\gamma_{\text{eff}}}, \quad \gamma_{\text{eff}} = -\frac{d \ln \chi(\tau)}{d \ln |\tau|}. \quad (2.13)$$

These effective exponents may be calculated theoretically from the flow equations, e.g.,

$$\eta_{\text{eff}}(l) = \gamma_{\phi}(u(l), v(l)), \quad (2.14)$$

$$\frac{1}{\nu_{\text{eff}}(l)} = 2 - \gamma_{m^2}(u(l), v(l)). \quad (2.15)$$

The variation of effective exponents depends on the RG flow in the parameter space as shown in Fig. 1.

## 2.2 Experiments

Experiments on site-diluted three-dimensional Ising magnets are usually performed on uniaxial disordered anti-ferromagnets such as  $\text{Fe}_{1-x}\text{Zn}_x\text{F}_2$  or  $\text{Mn}_{1-x}\text{Zn}_x\text{F}_2$ . The original aim was the study of the random-field behaviour when a uniform magnetic field is applied to such a disordered system. However, when the samples are of high quality (low mosaicity, high chemical homogeneity), also the behaviour in zero external magnetic field is accessible (3D disordered Ising model universality class). Staggered susceptibility and correlation length are deduced from neutron scattering experiments. The scattering intensity  $I(\mathbf{q})$  is the Fourier transform of the pair correlation function, where long-range fluctuations produce an isotropic Lorentzian peak centred at the superstructure spot position  $\mathbf{q}_0$  with a peak intensity given by the susceptibility and a width determined by the inverse correlation length, while long-range order gives a background proportional to the order parameter squared:

$$I(\mathbf{q}) = \langle m^2 \rangle \delta(\mathbf{q} - \mathbf{q}_0) + \frac{\chi}{1 + \xi^2(\mathbf{q} - \mathbf{q}_0)^2}. \quad (2.16)$$

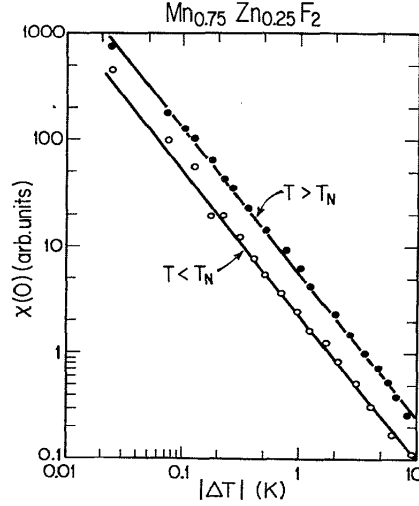


**Figure 2:** Neutron scattering measurements of the susceptibility in  $\text{Mn}_{0.75}\text{Zn}_{0.25}\text{F}_2$  close to criticality, governed by the disorder fixed point of the Ising model over the reduced temperature interval  $4 \times 10^{-4} < |T/T_c - 1| < 2 \times 10^{-1}$ . The solid lines show power-law fits with exponent  $\gamma = 1.364(76)$  above and below  $T_c$  (after Mitchell *et al.* [17]).

Fitting the Lorentzian at different temperatures eventually gives access to the physical quantities of interest, and further temperature analysis is required to get the critical exponents, critical amplitudes, and possibly the correction to scaling. For an example see Fig. 2.

### 2.3 Monte Carlo simulations

The majority of numerical studies of the disordered Ising model were concerned with site dilution. But we may also choose to model the disorder by bond dilution in order to compare these two kinds of disorder and to verify that they indeed lead to the same set of new critical exponents, as expected theoretically by universality. In our study we therefore considered the *bond-diluted* Ising model in three dimensions whose Hamiltonian with uncorrelated quenched random interactions can be written (in a Potts model normalisation) as

$$-\beta \mathcal{H} = \sum_{(i,j)} K_{ij} \delta_{\sigma_i, \sigma_j}, \quad (2.17)$$

where the spins take the values  $\sigma_i = \pm 1$  and the sum goes over all nearest-neighbour pairs  $(i, j)$ . The coupling strengths  $K_{ij}$  are drawn from the distribution

$$\mathcal{P}[K_{ij}] = \prod_{(i,j)} P(K_{ij}) = \prod_{(i,j)} [p \delta(K_{ij} - K) + (1 - p) \delta(K_{ij} - RK)]. \quad (2.18)$$

Besides bond dilution ( $R = 0$ ), which will be in the focus of the present paper, this also includes random-bond ferromagnets ( $0 < R < 1$ ) and the physically very different class of spin glasses ( $R = -1$ ) as special cases. For the here considered case of bond dilution, the couplings are thus allowed to take two different values  $K_{ij} = K \equiv J\beta \equiv J/k_B T$  and 0 with probabilities  $p$  and  $1 - p$ , respectively, with  $c = 1 - p$  being the concentration of missing bonds, which play the role of the non-magnetic impurities.

The phase diagram and the critical properties at a few selected dilutions were studied by large-scale Monte Carlo simulations on simple cubic lattices with  $V = L^3$  spins (up to  $L = 96$ ) and periodic boundary conditions in the three space directions, using the Swendsen-Wang cluster algorithm for updating the spins. All physical quantities are averaged over 2 000 – 5 000 disorder realisations, indicated by  $[\dots]_{\text{av}}$  (e.g.,  $[\chi]_{\text{av}}$  for the susceptibility). Standard definitions were used, e.g., for a given disorder realisation, the magnetisation is defined according to  $m = \langle |\mu| \rangle$  where  $\langle \dots \rangle$  stands for the thermal average and  $\mu = (N_{\uparrow} - N_{\downarrow}) / (N_{\uparrow} + N_{\downarrow})$  with  $N_{\uparrow, \downarrow}$  counting the number of “up” and “down” spins. The susceptibility follows from the fluctuation-dissipation relation,  $\chi = KV(\langle \mu^2 \rangle - \langle |\mu| \rangle^2)$ . The phase diagram is obtained by locating the maxima of the average susceptibility  $[\chi_L]_{\text{av}}$  (a diverging quantity in the thermodynamic limit) for increasing lattice sizes  $L$  as a function of the coupling strength  $K$ .

In disordered systems, the distributions of physical observables typically do not become sharper with increasing system size at a finite-randomness disorder fixed point. Rather their relative widths stay constant, a phenomenon called non-self-averaging. Non self-averaging can be quantitatively checked by evaluating the normalized squared width  $R_{\chi}(L) = V_{\chi}(L) / [\chi(L)]_{\text{av}}^2$ , where  $V_{\chi}$  is the variance of the susceptibility distribution:  $V_{\chi}(L) = [\chi(L)^2]_{\text{av}} - [\chi(L)]_{\text{av}}^2$ . This ratio is shown versus the inverse lattice size for three concentrations of the disordered Ising model in Fig. 3.

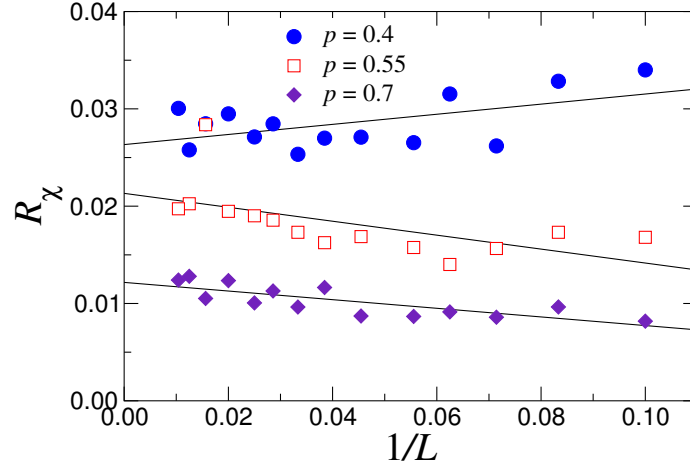


**Figure 3:** Normalized squared width of the susceptibility distribution versus the inverse of the lattice size for the three concentrations  $p = 0.4, 0.55,$  and  $0.7$  at the effective critical coupling  $K_c(L)$ . The straight lines are linear fits used as guides to the eye.

The fact that  $R_\chi$  approaches a constant when  $L$  increases as predicted by Aharony and Harris [18] is the signature of a non-self-averaging system, in agreement with the results of Wiseman and Domany [19, 20] for the site-diluted 3D Ising model.

As a function of the reduced temperature  $\tau = (K_c - K)$  ( $\tau < 0$  in the low-temperature (LT) phase and  $\tau > 0$  in the high-temperature (HT) phase) and the system size  $L$ , the susceptibility is expected to scale as

$$[\chi(\tau, L)]_{\text{av}} \sim |\tau|^{-\gamma} g_{\pm}(L^{1/\nu}|\tau|), \quad (2.19)$$

where  $g_{\pm}$  is a scaling function of the variable  $x = L^{1/\nu}|\tau|$  and the subscript  $\pm$  stands for the HT/LT phases. Recalling (2.13) we can define a temperature dependent effective critical exponent  $\gamma_{\text{eff}}(|\tau|) = -d \ln \bar{\chi} / d \ln |\tau|$ , which should converge towards the asymptotic critical exponent  $\gamma$  when  $L \rightarrow \infty$  and  $|\tau| \rightarrow 0$ . Our results for  $p = 0.7$  are shown in Fig. 4. For the greatest sizes, the effective exponent  $\gamma_{\text{eff}}(|\tau|)$  is stable around 1.34 when  $|\tau|$  is not too small, i.e., when the finite-size effects are not too strong. The plot of  $\gamma_{\text{eff}}(|\tau|)$  vs. the rescaled variable  $L^{1/\nu}|\tau|$  shows that the critical power-law behaviour holds in different temperature ranges for the different sizes studied. From the temperature behaviour of the susceptibility, we also have directly extracted the power-law exponent  $\gamma$  using error weighted least-squares fits by choosing the temperature range that gives the smallest  $\chi^2/\text{d.o.f}$  for several system sizes. The results are consistent with  $\gamma \approx 1.34 - 1.36$ .

From the previous expression of the susceptibility as a function of the reduced temperature and size, it is instructive to plot the scaling function  $g_{\pm}(x)$ . For finite size and  $|\tau| \neq 0$ , the scaling functions may be Taylor expanded in powers of the inverse scaling variable  $x^{-1} = (L^{1/\nu}|\tau|)^{-1}$ ,  $[\chi_{\pm}(\tau, L)]_{\text{av}} = |\tau|^{-\gamma} [g_{\pm}(\infty) + x^{-1} g'_{\pm}(\infty) + O(x^{-2})]$ , where the amplitude  $g_{\pm}(\infty)$  is usually denoted by  $\Gamma_{\pm}$ . Multiplying by  $|\tau|^{\gamma}$  leads to

$$[\chi_{\pm}(\tau, L)]_{\text{av}} |\tau|^{\gamma} = g_{\pm}(x) = \Gamma_{\pm} + O(x^{-1}). \quad (2.20)$$

When  $|\tau| \rightarrow 0$  but with  $L$  still larger than the correlation length  $\xi$ , one should recover the critical behaviour given by  $g_{\pm}(x) = O(1)$ . The critical amplitudes  $\Gamma_{\pm}$  follow, as shown in Fig. 4.

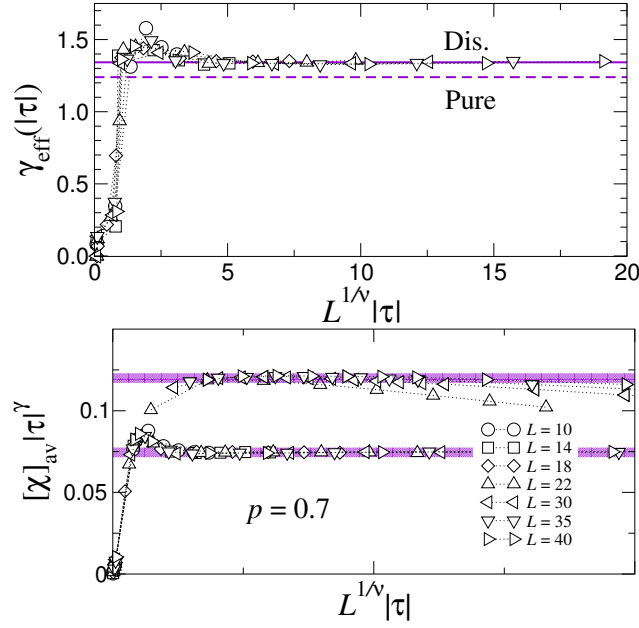


**Figure 4:** Variation of the temperature dependent effective critical exponent  $\gamma_{\text{eff}}(|\tau|) = -d \ln \bar{\chi} / d \ln |\tau|$  (in the low-temperature phase) as a function of the rescaled temperature  $L^{1/\nu}|\tau|$  (top) for the bond-diluted Ising model with  $p = 0.7$  and several lattice sizes  $L$ . The horizontal solid and dashed lines indicate the site-diluted and pure values of  $\gamma$ , respectively. The figure below shows the critical amplitudes  $\Gamma_{\pm}$  above and below the critical temperature.

## 2.4 High-temperature series expansions

Systematic series expansions [21] for statistical physics models defined on a lattice provide an useful complement to field-theoretical renormalization group studies and large-scale numerical Monte Carlo simulations. This is in particular true when studying phase transitions and critical phenomena of quenched, disordered systems. Series expansions techniques treat the quenched disorder average exactly and the infinite-volume limit is implicitly implied. Therefore one can obtain exact results up to a certain order in the inverse temperature for many quantities. Moreover, one can keep the disorder strength  $p$  as well as the dimension  $d$  as symbolic parameters and therefore analyse large regions of the parameter space of disordered systems. The critical part of the series expansion approach lies in the extrapolation techniques which are used in order to obtain information on the phase transition behaviour from the finite number of known coefficients. While for pure systems this usually works quite well, one can question the use of these extrapolation techniques in disordered systems, where the singularity structure of the free energy or susceptibility may be very complicated, involving Griffiths-type singularities or logarithmic corrections [22].

Based on the Hamiltonian (2.17), the combination

$$v_{ij} = \frac{e^{K_{ij}} - 1}{e^{K_{ij}} - 1 + q} \quad (2.21)$$

will be the relevant expansion parameter. For the Ising model ( $q = 2$ ) it simplifies to  $v_{ij} = \tanh(K_{ij}/2)$ . In the symmetric high-temperature phase, the susceptibility associated with the coupling  $\sum_i h_i (q \delta_{\sigma_i, 1} - 1) / (q - 1)$  to an external field  $h_i$  is given for a graph with  $N$  spins by summing over all two-point

correlations,

$$\chi = \frac{1}{N} \sum_i \sum_j \left[ \left\langle \frac{q \delta_{\sigma_i, \sigma_j} - 1}{q - 1} \right\rangle \right]_{\text{av}}. \quad (2.22)$$

The brackets  $[\dots]_{\text{av}}$  indicate the quenched disorder average with respect to the distribution (2.18).

#### 2.4.1 Series generation methodology

There are a couple of well-established methods [21] known for the systematic generation of high-temperature series (HTS) expansions which differ in the way relevant subgraphs are selected or grouped together. We employed the star-graph method which can be adopted to systems involving quenched disorder [23, 24] (as also can the no-free-end method [25]) since it allows one to take the disorder average on the level of individual graphs. The basic idea is to assemble the value of some extensive thermodynamic quantity  $F$  on a large or even infinite graph from its values on subgraphs: Graphs constitute a partially ordered set under the “subgraph” relation. Therefore, for every function  $F(G)$  defined on the set of graphs exists another function  $W_F(G)$  such that  $F(G) = \sum_{g \subseteq G} W_F(g)$ , for all graphs  $G$ . This function can be calculated recursively via  $W_F(G) = F(G) - \sum_{g \subset G} W_F(g)$ , resulting for an infinite (e.g. hypercubic) lattice in  $F(\mathbb{Z}^d) = \sum_G (G : \mathbb{Z}^d) W_F(G)$ , where  $(G : \mathbb{Z}^d)$  denotes the weak embedding number of the graph  $G$  in the given lattice structure [26].

The following observation makes this a useful method: A vertex is termed articulation point if the deletion of the vertex renders the graph disconnected. The “star graphs” which gave the method its name are defined by the absence of such articulation points. Now let  $G$  be a graph with an articulation vertex where two star subgraphs  $G_{1,2}$  are glued together. Then  $W_F(G)$  vanishes if  $F(G) = F(G_1) + F(G_2)$ . An observable  $F$  for which this property is true on arbitrary graphs with articulation points allows a star-graph expansion. All non-star graphs have zero weight  $W_F$  in the sum for  $F(\mathbb{Z}^d)$ . It is easy to see that the (properly normalized) free energy  $\log Z$  has this property and it can be proved [24] that the inverse susceptibility  $1/\chi$  has it, too, even for arbitrary inhomogeneous couplings  $K_{ij}$ . This restricts the summation for  $F(\mathbb{Z}^d)$  to a sum over star graphs. The linearity of the recursion relations then enables the calculation of quenched averages over the coupling distribution on the level of individual graphs. The resulting recipe for the susceptibility series is:

- Graph generation and embedding number counting.
- Calculation of  $Z(G)$  and the correlation matrix  $M_{nm}(G) = \text{Tr}(q \delta_{\sigma_n, \sigma_m} - 1) e^{-\beta \mathcal{H}(\{\sigma_{ij}\})}$  for all graphs as polynomials in  $E$  variables  $v_{ij}$  defined in (2.21).
- Inversion of the  $Z$  polynomial as a series up to the desired order.
- Averaging over quenched disorder,  $N_{nm}(G) = [M_{nm}/Z]_{\mathcal{P}(K)}$ , resulting in a matrix of polynomials in  $(p, v)$ .
- Inversion of the matrix  $N_{nm}$  and subgraph subtraction,  $W_\chi(G) = \sum_{n,m} (N^{-1})_{nm} - \sum_{g \subset G} W_\chi(g)$ .
- Collecting the results from all graphs,  $1/\chi = \sum_G (G : \mathbb{Z}^d) W_\chi(G)$ .

**Table 1:** Number of star graphs with  $E \geq 8$  links and non-vanishing embedding numbers on  $\mathbb{Z}^d$ . For  $E = 1, 4, 6,$  and  $7$  only a single star graph exists.

order $E$	8	9	10	11	12	13	14	15	16	17	18	19
#	2	3	8	9	29	51	142	330	951	2561	7688	23078

Algorithmically the most cumbersome part of this recipe is the first step, the generation of star graphs and calculation of their (weak) embedding numbers. The graph generation is usually done by recursively adding nodes and edges to a list of smaller graphs. To make sure that no double counting occurs this requires an isomorphism test, i.e., the decision whether two given adjacency lists or adjacency matrices describe the same graph modulo relabelling and reordering of edges and nodes. We employed the NAUTY package by McKay [27] which allows very fast isomorphism tests by calculating a canonical representation of the automorphism group of the graphs. By this means, we classified for the first time all star graphs up to order 19 that can be embedded in hypercubic lattices, see Table 1. As with any series expansion, the effort grows exponentially with the maximal order of the expansion, rendering each new order roughly as “expensive” as all previous orders taken together. This is illustrated in Fig. 5 where already the number of star graphs is seen to grow exponentially as a function of the links  $E$ . The exponential fit in the range  $E = 13 - 19$  suggests that the number of star graphs increases roughly by a factor of 2.8 in each of the next higher orders, predicting about 65 000 different star graphs with  $E = 20$  and about 180 000 with  $E = 21$ .

For each of these graphs we calculated their (weak) embedding numbers for  $d$ -dimensional hypercubic lattices (up to order 17 for arbitrary  $d$ , order 18 (general  $q$ -state Potts) and 19 (Ising) for dimensions  $d \leq 5$ ). Two typical results are depicted in Fig. 6. For the embedding count we implemented a refined version of the backtracing algorithm by Martin [26], making use of a couple of simplifications for bipartite hypercubic lattices  $\mathbb{Z}^d$ . After extensive tests to find the optimal algorithm for the “innermost” loop, the test for collisions in the embedding, we ended up using

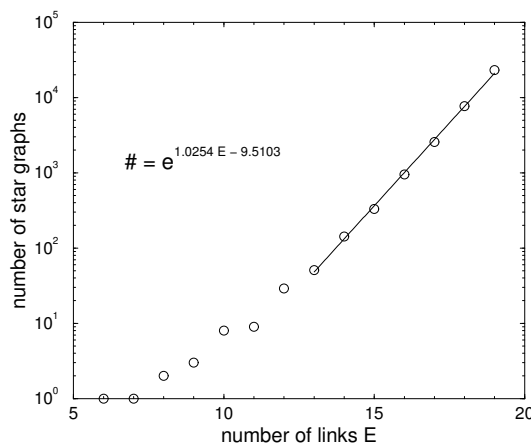
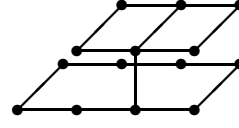
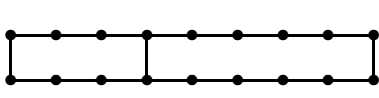


**Figure 5:** Growth behaviour of the number of star graphs with  $E$  links that can be embedded in hypercubic lattices  $\mathbb{Z}^d$ .

POS (LATT2005) 018



$$7620 \binom{d}{2} + 76851600 \binom{d}{3} + 14650620864 \binom{d}{4} \\ + 404500471680 \binom{d}{5} + 3355519311360 \binom{d}{6}$$

$$12048 \binom{d}{3} + 396672 \binom{d}{4} + 2127360 \binom{d}{5} + 2488320 \binom{d}{6}$$

**Figure 6:** Two star graphs of order 17 and 19 and their weak embedding numbers up to 6 dimensions.

optimized hash tables.

The second step of the series generation requires the exact calculation of the partition function and the matrix of correlations  $M_{nm}$  for each star graph with arbitrary symbolic couplings  $J_{ij}$  defined on the  $E \leq 19$  edges. The crucial observation is that this can be done most efficiently by using the cluster representation

$$Z \propto \mathcal{Z} = q^{-N} \text{Tr} \prod_{\langle ij \rangle} [1 - v_{ij} + v_{ij} q \delta_{\sigma_i, \sigma_j}] \\ = \sum_C q^{e+c-N} \left( \prod_{\langle ij \rangle \in C} v_{ij} \right) \left( \prod_{\langle ij \rangle \notin C} (1 - v_{ij}) \right), \quad (2.23)$$

where the sum goes over all clusters  $C \subseteq G$ ,  $e$  is the number of links of the cluster and  $c$  the number of connected components of  $C$ . The reduced partition function  $\mathcal{Z} \equiv Z q^{E-N} / \prod_{\langle ij \rangle} (e^{K_{ij}} - 1 + q)$  is normalized such that  $\log \mathcal{Z}$  has a star-graph expansion. Similarly, the calculation of the susceptibility involves the matrix of correlations

$$M_{nm} \propto \sum_{C_{nm}} q^{e+c-N} \left( \prod_{\langle ij \rangle \in C} v_{ij} \right) \left( \prod_{\langle ij \rangle \notin C} (1 - v_{ij}) \right), \quad (2.24)$$

where the sum is restricted to all clusters  $C_{nm} \subseteq G$  in which the vertices  $n$  and  $m$  are connected.

This representation essentially reduces the summation over  $q^N$  states to a sum over  $2^E$  clusters which, compared with previous implementations, results in a huge saving factor in computing time (of the order of  $10^6$ ). Further improvements result if the  $2^E$  clusters belonging to a graph are enumerated by Gray codes [28] such that two consecutive clusters in the sum (2.23) differ by exactly one (added or deleted) link. In the Ising case  $q = 2$  another huge simplification takes place since only clusters where all vertices are of even degree contribute to the cluster sum.

Since general purpose software for symbolic manipulations turned out to be too slow for our purposes, we developed a C++ template library using an expanded degree-sparse representation of polynomials and series in many variables. For arbitrary-precision arithmetics the open source library GMP was used. Finally, for the case of bond dilution ( $R = 0$  in (2.18)) considered here, we made use of the fact that the disorder average is most easily calculated via

$$[v_1^{n_1} \dots v_k^{n_k}]_{\text{av}} = p^k v_0^{n_1 + \dots + n_k}. \quad (2.25)$$

## 2.4.2 Series analysis: techniques and results

Our high-temperature series expansion for the susceptibility up to order 19 is given with coefficients as polynomials in  $p$ ,  $\chi(v) = \sum_n a_n(p) v^n$  [29, 30]. Therefore it should be well-suited for the

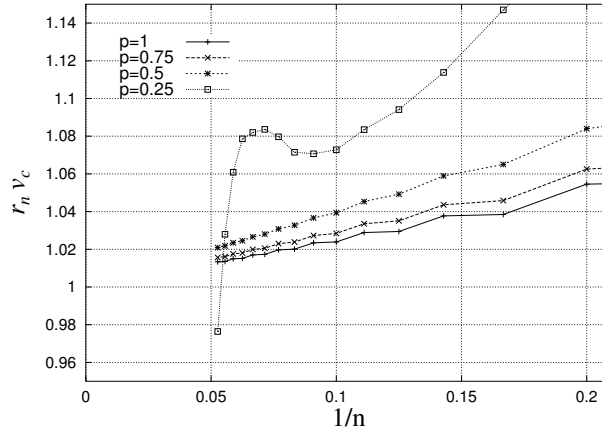


**Figure 7:** Ratio approximations for different dilutions  $p$  vs.  $1/n$ . In order to make them visually comparable, they are (except for  $p = 0.25$ ) normalized by their respective critical couplings  $v_c$ .

method of partial differential approximants [31] which was successfully used to analyse series with an anisotropy parameter describing the crossover between 3D Ising, XY and Heisenberg behaviour [32]. But this method was unable to give conclusive results. Therefore we confined ourselves to a single-parameter series for selected values of  $p$ .

The ratio method assumes that the expected singularity of the form

$$\chi(v) = A(v_c - v)^{-\gamma} + \dots \quad (2.26)$$

is the closest to the origin. Then the consecutive ratios of series coefficients behave asymptotically as

$$r_n = \frac{a_n}{a_{n-1}} = v_c^{-1} \left( 1 + \frac{\gamma-1}{n} \right). \quad (2.27)$$

Figure 7 shows these ratios for different values of  $p$ . For  $p$  close to 1 they show the typical oscillations related to the existence of an antiferromagnetic singularity at  $-v_c$ . Near the percolation threshold at  $p_c = 0.248812$  [33] (where  $T_c$  goes to 0,  $v_c$  to 1) the series is clearly ill-behaved, related to the  $\exp(1/T)$  singularity expected there. Besides that, the slope (related to  $\gamma$ ) is decreasing with  $p$ .

The widely used DLog-Padé method consists in calculating Padé approximants to the logarithmic derivative of  $\chi(v)$ ,

$$\frac{d \ln \chi(v)}{dv} = \frac{\gamma}{v_c - v} + \dots \quad (2.28)$$

The smallest real pole of the approximant is an estimation of  $v_c$  and its residue gives  $\gamma$ . The results presented in Table 2 are the averages of 45 – 55 different Padé approximants for each value of  $p$ , with the error in parentheses indicating the standard deviation. The scattering of the Padé approximants increases with decreasing  $p$ , getting again inconclusive near the percolation threshold. Nevertheless, down to about  $p = 0.4$  the series estimates for  $v_c$  respectively  $T_c$  are in perfect agreement with the Monte Carlo (MC) results of Ref. [34]. This is demonstrated in Fig. 8 where also the (properly normalized) mean-field and effective-medium approximation [35] are shown for comparison.

**Table 2:** Transition points  $v_c = \tanh(K_c/2)$  and critical exponents  $\gamma$  for different dilutions  $p$  as obtained from DLog-Padé approximants.

$p$	$v_c$	$\gamma$
1	0.21813(1)	1.2493(7)
0.85	0.25788(1)	1.2714(8)
0.7	0.31566(2)	1.305(4)
0.55	0.40743(10)	1.365(6)
0.4	0.576(1)	1.435(60)

The critical exponent  $\gamma$ , as provided by this method, apparently varies with the disorder strength. More sophisticated analysis methods, such as inhomogeneous differential approximants [36, 37], the Baker-Hunter method [38] or the methods M1 and M2 [39], especially tailored to deal with confluent singularities as one would expect in a crossover situation, give improved results in the pure ( $p = 1$ ) case but do not essentially change the results in the presence of disorder.

Thus, while for theoretical reasons we still find it likely that the variation of  $\gamma$  with the disorder strength can be attributed to neglected or insufficiently treated correction terms, it proved clearly impossible to verify this effect in the series analysis. In fact, a plot of  $\gamma$  vs.  $p$  does not even show an indication of a plateau. In the central disorder regime,  $p = 0.5 - 0.7$ , the high-temperature series estimates given in Table 2 are at least compatible with Monte Carlo results for site and bond dilution [34, 40, 41] which cluster quite sharply around  $\gamma_{MC} = 1.34(1)$ . Field-theoretic renormalization group estimates [42, 15] favor slightly smaller exponents of  $\gamma_{RG} = 1.32 - 1.33$ , while experiments [10, 17, 43] report values between  $\gamma_{exp} = 1.31 - 1.44$ , cp., e.g., Table 3 (see also Ref. [44]).

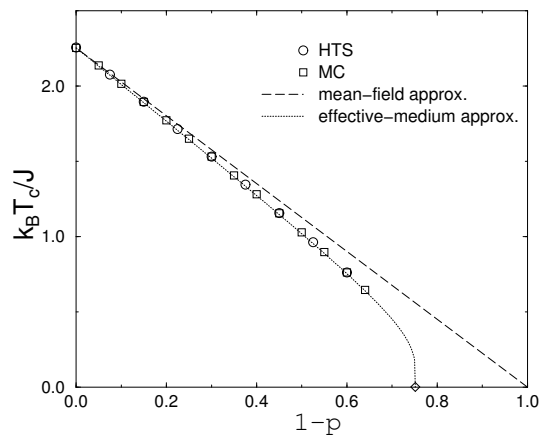


**Figure 8:** Transition temperatures of the bond-diluted Ising model for different dilutions  $p$  as obtained from our DLog-Padé high-temperature series (HTS) analyses and from Monte Carlo (MC) simulations [34]. For comparison also the (properly normalized) mean-field and effective-medium approximations are shown.

**Table 3:** Critical exponents and critical amplitude ratio of the susceptibility as measured with different techniques.

Technique	$\gamma$	$\Gamma_+/\Gamma_-$	$\omega$	Ref.
RG		2.2		[45]
	1.318		0.39(4)	[46, 42] <sup>1</sup>
	1.330(17)		0.25(10)	[15] <sup>2</sup>
Neutron scattering	1.44(6)	2.2	0.5	[10] <sup>3</sup>
	1.31(3)	2.8(2)		[43] <sup>4</sup>
	1.37(4)	2.40(2)		[17] <sup>5</sup>
MC	1.342(10)		0.37	[47] <sup>6</sup>
	1.34(1)	1.62(10)	undetermined	[34] <sup>7</sup>
	1.342(7)		undetermined	[40] <sup>8</sup>
	1.314(4)	1.67(15)	undetermined	[48] <sup>9</sup>
HTS	1.305(4)		undetermined	[49] <sup>10</sup>

<sup>1</sup> 4 loop approximation.<sup>2</sup> 6 loop approximation, fixed dimension.<sup>3</sup>  $\text{Fe}_{1-x}\text{Zn}_x\text{F}_2$ ,  $x = 0.4, 0.5$ ,  $|\tau| \sim 10^{-2}$ .<sup>4</sup>  $\text{Fe}_{0.46}\text{Zn}_{0.54}\text{F}_2$ ,  $1.5 \times 10^{-3} \leq |\tau| \leq 10^{-1}$ .<sup>5</sup>  $\text{Mn}_{0.75}\text{Zn}_{0.25}\text{F}_2$ ,  $4 \times 10^{-4} \leq |\tau| \leq 2 \times 10^{-1}$ .<sup>6</sup> site dilution,  $p = 0.4$  to  $0.8$ .<sup>7</sup> bond dilution,  $p = 0.7$ . The correction to scaling is too small to be determined.<sup>8</sup> site dilution,  $p = 0.8$ . The observed correction to scaling could be the next-to-leading one.<sup>9</sup> site dilution,  $p = 0.8$ .<sup>10</sup> bond dilution,  $p = 0.7$ .

### 3. Disordered 4-state Potts model

#### 3.1 Monte Carlo simulations

Let us now turn to the 4-state Potts model which exhibits a rather strong first-order phase transition in the pure case. In order to map out the phase diagram of the diluted model we considered all concentrations  $p$  in the interval  $[0.28, 1]$  in steps of 0.04 and determined again the locations of the maxima of the susceptibility for a given lattice size  $L$ . The resulting phase diagram is again in very good agreement with the effective-medium approximation, here with [50, 51]  $K_c(1) = 0.62863(2)$ , and estimates from high-temperature series expansions [49].

In a second step, the order of the phase transitions was investigated. To satisfy our criterion  $N_{\text{MCS}} > 250 \tau_e$ , here the number of MC sweeps had to be increased to much larger values (up to 15000 – 30000) than in the Ising case. In fact, a first indication for a crossover between first- and second-order transitions with decreasing dilution  $p$  could be derived from the autocorrelation times. In the first-order regime we performed multibondic simulations [52, 53] and estimated the interface tension from

$$\sigma_{od} = \frac{1}{2L^2} \log \frac{P_{\max}}{P_{\min}}, \quad (3.1)$$

where  $P_{\max}$  is the maximum of the probability density reweighted to the temperature where the two peaks are of equal height, and  $P_{\min}$  is the minimum in between, see Fig. 9. The linear extrapolations of  $\sigma_{od}$  in  $1/L$  in the lower part of Fig. 9 imply non-vanishing interface tensions only for  $p = 0.84$  and above. For  $p \leq 0.76$ ,  $\sigma_{od}$  seems to vanish in the infinite-volume limit, being indicative of the expected softening to a second-order phase transition. The tricritical point would thus be located around  $p = 0.76 - 0.84$ , in good agreement with the estimate of  $p = 0.80$  derived from our analysis of autocorrelation times.

Below this concentration, the system exhibits a second-order transition. This is signaled qualitatively by typical single-peak order-parameter probability distributions at the transition temperature. To confirm the softening to second-order phase transitions for  $p \leq 0.76$  we performed a detailed FSS [50] study at  $p = 0.56$  with lattice sizes ranging up to  $L = 96$  and the number of realisations varying between 2 000 and 5 000. As can be inspected in Fig. 10, the variance of the  $\chi_{[J]}$  measurements is somewhat larger than in the Ising model and the distribution exhibits a long tail towards large susceptibilities, reflecting the first-order like signal of a few rare-events.

The choice of  $p = 0.56$  is motivated by our observation that in this range of dilutions the corrections to asymptotic FSS of the effective transition points are minimal. The log-log plot for  $[\chi]_{\text{av,max}}$  in Fig. 11 indeed suggests that for this quantity the corrections become quite small above  $L = 30$ , and fits of the form  $a_\chi L^{\gamma/\nu}$  starting at  $L_{\min} > 30$  yield  $\gamma/\nu = 1.50(2)$ . Using the data

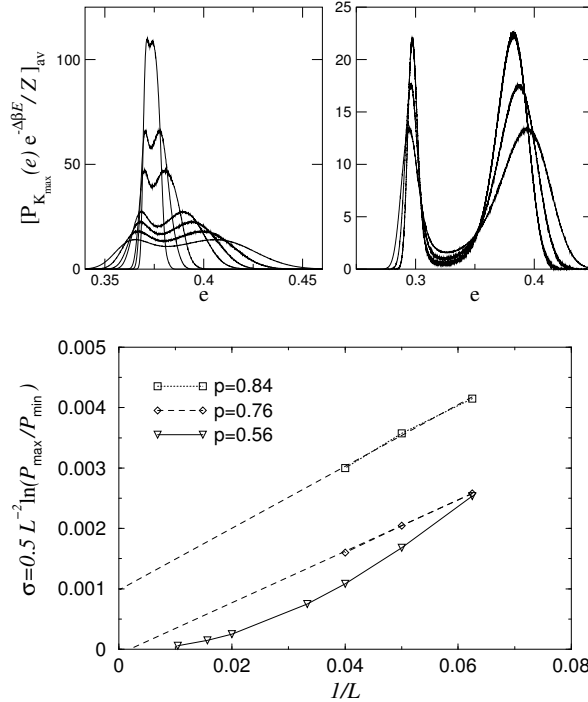


**Figure 9:** Probability density of the energy of the 3D bond-diluted 4-state Potts model reweighted to equal peak height for  $p = 0.56$  (top left) and  $p = 0.84$  (top right). Interface tension versus inverse lattice size (bottom).

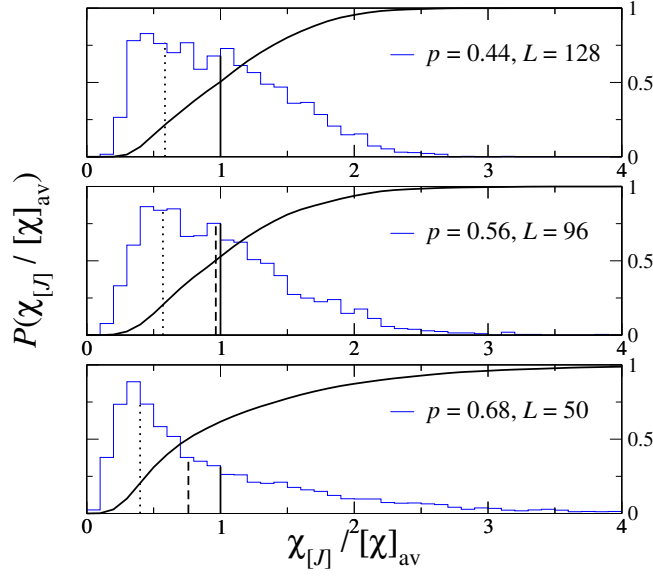


**Figure 10:** Probability distribution of the susceptibility  $\chi_{[J]}(K_{\max})$  for the bond concentrations  $p = 0.44$ ,  $0.56$ , and  $0.68$  for the largest lattice size in each case. The full curve represents the integrated distribution. At each dilution, a full vertical line shows the location of the average susceptibility, a dashed line shows the median and a dotted line shows the average over the events which are smaller than the median.

for  $L < 30$  only, on the other hand, we obtained perfect fits assuming percolation exponents [33],  $\gamma/\nu \approx 2.05$ , cf. Fig. 11. Similarly, the FSS of the quantity  $(d \ln[m]_{\text{av}}/dK)_{K_{\max}} \propto L^{1/\nu}$  gives for  $L_{\min} > 30$  an estimate of the exponent  $1/\nu = 1.33(3)$ , consistent with the stability condition [54]  $1/\nu \leq d/2 = 1.5$  at the disorder fixed point. The same procedure was applied to the magnetisation  $[m_{K_{\max}}]_{\text{av}} \propto L^{-\beta/\nu}$ , but here the associated critical exponent turned out to be not yet stable. We therefore also considered the FSS behaviour of higher (thermal) moments of the magnetisation,  $[\langle \mu^n \rangle]_{\text{av}}$ , which should scale with an exponent  $n\beta/\nu$ . The results for the first moments exhibit, however, again much stronger corrections to scaling than we observed for  $[\chi]_{\text{av}}$  or  $[d \ln m/dK]_{\text{av}}$ , leading to quite a conservative final estimate of  $\beta/\nu = 0.65(5)$ . We nevertheless note that our results do not fit satisfactorily the hyperscaling law  $2\beta/\nu = d - \gamma/\nu$ . The reason could be strong corrections-to-scaling at the disorder fixed point which are hard to cope with for medium-sized systems [50].

### 3.2 High-temperature series expansions

As expected theoretically and clearly confirmed by our Monte Carlo results, from a certain finite disorder strength on the three-dimensional 4-state Potts model gets softened to a second-order transition governed by a disorder fixed point. In the latter regime we are interested in locating power-law divergences of the form (2.26) from our susceptibility series up to order 18 [55, 49, 30]. To localize a first-order transition point, however, a high-temperature series alone is not sufficient since there the correlation length remains finite and no critical singularity occurs. In analysing series by ratio, Padé or differential approximants, the approximant will provide an analytic continuation of the thermodynamic quantities beyond the transition point into a metastable region on

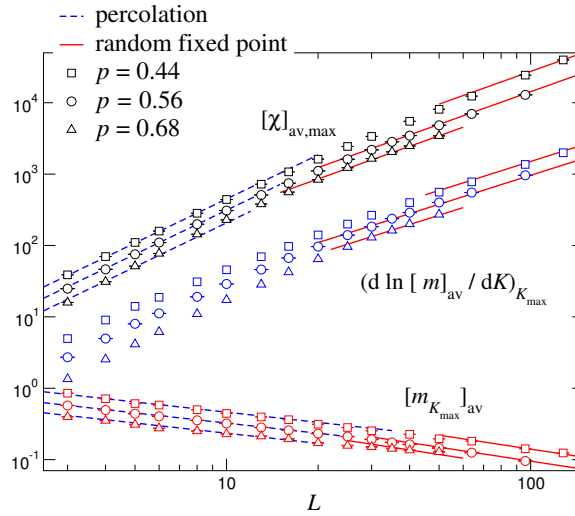


**Figure 11:** FSS behaviour of the susceptibility maxima as well as of  $d \ln [m]_{\text{av}} / dK$  and the magnetisation at  $K_{\text{max}}$  for the 3D bond-diluted 4-state Potts model at three dilutions (with vertical offsets added for the sake of clarity). The scaling behaviour for small lattice sizes below a crossover length scale is presumably governed by the percolation fixed point, indicated by the dashed lines.

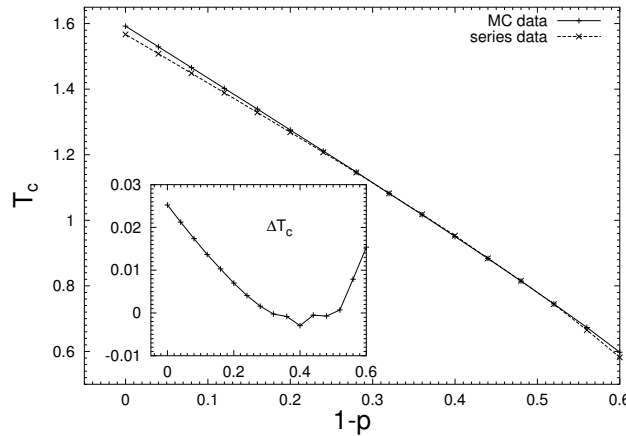


**Figure 12:** Transition temperatures of the bond-diluted 4-state Potts model for different dilution  $p$  as obtained from Monte Carlo (MC) simulations [50] and DLog-Padé series analyses. The inset shows the difference between the two estimates.

a pseudo-spinodal line with a singularity  $T_c^* < T_c$  and effective “critical exponents” at  $T_c^*$ . Again we first employed the ratio method which behaves qualitatively similar to the Ising model case (oscillations caused by the antiferromagnetic singularity at  $-v_c$ , strong influence of the percolation point at  $p_c \approx 0.25$ ). The slope ( $\propto \gamma - 1$ ) was found to decrease with  $p$ , changing from  $\gamma < 1$  to  $\gamma > 1$  around  $p = 0.5$ .

Figure 12 compares the critical temperature, estimated from an average of 25 – 30 Padé approximants for each value of  $p$ , with the results of recent Monte Carlo simulations [50]. For  $p$  close to 1, in the first-order region, the series underestimates the critical temperature. As explained

above, this is an estimate not of  $T_c$  but of  $T_c^*$ . Between  $p = 0.7$  and  $p = 0.5$ , the estimates confirm, within errors, the Monte Carlo results, indicating that now both methods see the same second-order transition. Beyond  $p = 0.5$ , the scatter of different Padé approximants increases rapidly, related to the crossover to the percolation point.

The situation is more complicated with respect to the critical exponent  $\gamma$ . The DLog-Padé analysis gives inconclusive results due to a large scattering between different Padé approximants. One possible reason for this failure is the existence of confluent singularities. The dots in Eq. (2.26) indicate correction terms which can be parametrized as follows:

$$\chi(v) = A(v_c - v)^{-\gamma} [1 + A_1(v_c - v)^{\Delta_1} + A_2(v_c - v)^{\Delta_2} + \dots], \quad (3.2)$$

where  $\Delta_i$  are the confluent correction exponents. Among the various sophisticated analysis methods (inhomogeneous differential approximants [36, 37] and the methods M1 and M2 [39]), in the case at hand, the Baker-Hunter method [38] appeared to be the most successful, giving consistent results at larger dilutions  $p < 0.65$  where the leading-term DLog-Padé analysis failed. The Baker-Hunter method assumes that the function under investigation has confluent singularities

$$F(z) = \sum_{i=1}^N A_i \left(1 - \frac{z}{z_c}\right)^{-\lambda_i} = \sum_{n=0}^{\infty} a_n z^n, \quad (3.3)$$

which can be transformed into an auxiliary function  $g(t)$  that is meromorphic and therefore suitable for Padé approximation. After the substitution  $z = z_c(1 - e^{-t})$  we expand  $F(z(t)) = \sum_n c_n t^n$  and construct the new series

$$g(t) = \sum_{n=0}^{\infty} n! c_n t^n = \sum_{i=1}^N \frac{A_i}{1 - \lambda_i t}, \quad (3.4)$$

such that Padé approximants to  $g(t)$  exhibit poles at  $t = 1/\lambda_i$  with residues  $-A_i/\lambda_i$ . This method is applied by plotting these poles and residues for different Padé approximants to  $g(t)$  as functions of  $z_c$ . The optimal set of values for the parameters is determined visually from the best clustering of different Padé approximants.

Using this method, our results for the critical exponent  $\gamma$  are plotted in Fig. 13. They show an effective exponent monotonically decreasing with  $p$  but reaching a plateau at  $\gamma = 1$  for dilutions between  $p = 0.58$  and  $p = 0.54$ . The following sharp increase is to be interpreted as due to the crossover to the percolation fixed point at  $p_c \approx 0.25$ ,  $T_c = 0$ , where a  $\chi \sim \exp(1/T)$  behaviour is expected.

It is well known (see, e.g., Ref. [56]) that series analysis in crossover situations is extremely difficult. If the parameter  $p$  interpolates between regions governed by different fixed points, the exponent obtained from a finite number of terms of a series expansion must cross somehow between its universal values, and does this usually quite slowly. Therefore it does not come as a surprise that the Monte Carlo simulations quoted above see the onset of a second order phase transition already for smaller values of the disorder strength  $1 - p$ . The mere existence of a plateau in  $\gamma_{\text{eff}}(p)$ , however, is an indication that here truly critical behaviour is seen. It is governed by a fixed point for which we obtain  $\gamma = 1.00(3)$ . Here, as always in series analyses, the error estimates the scattering of different approximants.

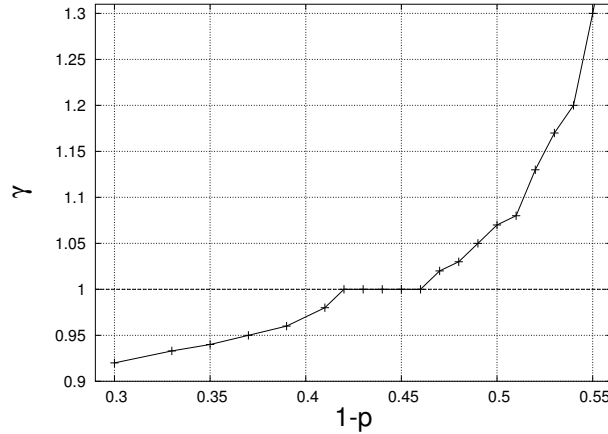


**Figure 13:** Effective critical exponent  $\gamma$  as function of the dilution  $p$  from Baker-Hunter analyses.

#### 4. Summary

By performing large-scale Monte Carlo simulations we have investigated the influence of bond dilution on the critical properties of the 3D Ising and 4-state Potts models. In the 3D Ising case the universality class of the disordered model is modified by disorder but its precise characterisation turned out to be difficult because of the competition between the different fixed points which induce crossover effects, even for relatively large lattice sizes. Overall, however, our results clearly demonstrate universality between site- and bond-dilution, and the critical exponent estimates are compatible with those obtained with completely alternative techniques such as renormalization group studies and high-temperature series expansions.

One generic problem of the numerical approach is the computation of quenched averages which requires simulations of many different disorder realizations. With high-temperature series expansions, on the other hand, this average can be calculated exactly and, keeping the relevant parameters as symbolic variables, whole phase diagrams can be scanned systematically. Based on our comprehensive toolbox for generating and enumerating star graphs, we have presented analyses of the susceptibility series for both disordered models. The phase diagrams in the  $p$ - $T$ -plane are found in very good agreement with the Monte Carlo results. For the critical exponent  $\gamma$  of the 3D bond-diluted Ising model, however, large crossover effects render a reliable determination from series expansions up to order 19 very difficult. Our estimates are clearly different from the pure case but exhibit quite a pronounced dependence on the degree of dilution.

Applying the simulational approach to the 3D 4-state Potts model with its strong first-order phase transition in the pure case, we obtained clear evidence for softening to a continuous transition at strong disorder, with estimates for the critical exponents of  $\nu = 0.752(14)$ ,  $\gamma = 1.13(4)$ , and  $\beta = 0.49(5)$  at  $p = 0.56$ . The analysis of both the autocorrelation time [50, 51] and the interface tension leads to the conclusion of a tricritical point around  $p = 0.80$ . By comparing our high-temperature series expansions with the numerical data we can identify signals for softening at a finite disorder strength also within this approach, but due to the more complicated singularity structure in this case, series analyses are rather involved.

## References

- [1] A. B. Harris, *Effect of random defects on the critical behaviour of Ising models*, Journal of Physics C: Solid State Physics **7**, 1671 (1974).
- [2] Y. Imry and M. Wortis, *Influence of quenched impurities on first-order phase transitions*, Phys. Rev. B **19**, 3580 (1979).
- [3] M. Aizenman and J. Wehr, *Rounding of first-order phase transitions in systems with quenched disorder*, Phys. Rev. Lett. **62**, 2503 (1989).
- [4] K. Hui and A. N. Berker, *Random-field mechanism in random-bond multicritical systems*, Phys. Rev. Lett. **62**, 2507 (1989).
- [5] J. Cardy and J. L. Jacobsen, *Critical behaviour of random-bond Potts models*, Phys. Rev. Lett. **79**, 4063 (1997).
- [6] C. Chatelain and B. Berche, *Finite-size scaling study of the surface and bulk critical behavior in the random-bond eight-state Potts model*, Phys. Rev. Lett. **80**, 1670 (1998).
- [7] D. E. Khmel'nitskiĭ, *Second-order phase transition in inhomogeneous bodies*, Sov. Phys. JETP **41**, 981 (1974).
- [8] R. Folk, Yu. Holovatch, and T. Yavors'kii, *Critical exponents of a three dimensional weakly diluted quenched Ising model*, Physics-Uspekhi **46**, 169 (2003).
- [9] A. Pelissetto and E. Vicari, *Critical phenomena and renormalization-group theory*, Phys. Rep. **368**, 549 (2002).
- [10] R. J. Birgeneau, R. A. Cowley, G. Shirane, and H. Yoshizawa, *Phase transitions in diluted magnets: critical behaviour, percolation, and random fields*, J. Stat. Phys. **34**, 817 (1984).
- [11] D. P. Belanger, *Experimental characterization of the Ising model in disordered antiferromagnets*, Braz. J. Phys. **30**, 682 (2000).
- [12] D. P. Landau, *Critical behavior of the simple cubic Ising model with quenched site impurities*, Phys. Rev. B **22**, 2450 (1980).
- [13] W. Janke, P.-E. Berche, C. Chatelain, and B. Berche, *Phase transitions in disordered ferromagnets*, in *NIC Symposium 2004*, D. Wolf, edited by G. Münster and M. Kremer, NIC Series, Vol. 20, pp. 241 – 250 (2003).
- [14] D. V. Pakhnin and A. I. Sokolov, *Critical exponents for a three-dimensional impure Ising model in the five-loop approximation*, Sov. Phys. JETP Lett. **71**, 412 (2000).
- [15] A. Pelissetto and E. Vicari, *Randomly dilute spin models: A six-loop field-theoretic study*, Phys. Rev. B **62**, 6393 (2000).
- [16] Yu. Holovatch, V. Blavats'ka, M. Dudka, C. von Ferber, R. Folk, and T. Yavors'kii, *Weak quenched disorder and criticality: resummation of asymptotic(?) series*, Int. J. Mod. Phys. B **16**, 4027 (2002).
- [17] P. W. Mitchell, R. A. Cowley, H. Yoshizawa, P. Böni, Y. J. Uemura, and R. J. Birgeneau, *Critical behavior of the three-dimensional site-random Ising magnet:  $Mn_xZn_{1-x}F_2$* , Phys. Rev. B **34**, 4719 (1986).
- [18] A. Aharony and A. B. Harris, *Absence of self-averaging and universal fluctuations in random systems near critical points*, Phys. Rev. Lett. **77**, 3700 (1996).

- [19] S. Wiseman and E. Domany, *Finite-size scaling and lack of self-averaging in critical disordered systems*, Phys. Rev. Lett. **81** 22 (1998).
- [20] S. Wiseman and E. Domany, *Self-averaging, distribution of pseudocritical temperatures, and finite size scaling in critical disordered systems*, Phys. Rev. E **58** 2938 (1998).
- [21] C. Domb and M. S. Green, eds., *Series Expansions for Lattice Models*, vol. 3 of *Phase Transitions and Critical Phenomena* (Academic Press, New York, 1974).
- [22] J. Cardy, *Logarithmic correlations in quenched random magnets and polymers*, preprint cond-mat/9911024.
- [23] D. C. Rapaport, *The Ising ferromagnet with impurities: A series expansion approach. I and II*, Journal of Physics C: Solid State Physics **5**, 1830, 2813 (1972).
- [24] R. R. P. Singh and S. Chakravarty, *High-temperature series expansion for spin glasses. I. Derivation of the series*, Phys. Rev. B **36**, 546 (1987).
- [25] A. B. Harris, *Renormalized  $(1/\sigma)$  expansion for lattice animals and localization*, Phys. Rev. B **26**, 337 (1982).
- [26] J. L. Martin, *Computer techniques for evaluating lattice constants*, in Ref. [21], pp. 97 – 112.
- [27] B. D. McKay, *Practical graph isomorphism*, Congressus Numerantium **30**, 45 (1981).
- [28] W. H. Press, S. A. Teukolsky, W. T. Vetterling, and B. P. Flannery, *Numerical Recipes in C* (Cambridge University Press, Cambridge, 1992).
- [29] M. Hellmund and W. Janke, *High-temperature series expansions for random-bond Potts models on  $\mathbb{Z}^d$* , Comp. Phys. Comm. **147**, 435 (2002).
- [30] M. Hellmund and W. Janke, *High-temperature series expansions for random Potts models*, Condens. Matter Phys. **8**, 59 (2005).
- [31] M. E. Fisher and J.-H. Chen, *Bicriticality and partial differential approximants*, in *Phase Transitions: Cargèse 1980*, edited by M. Lévy, J. C. Le Guillou, and J. Zinn-Justin (Plenum, New York, 1982), pp. 169–216.
- [32] Z. Salman and J. Adler, *Series analysis of tricritical behaviour: Mean-field model and partial differential approximants*, Journal of Physics A: Mathematical and General **30**, 1979 (1997).
- [33] C. D. Lorenz and R. M. Ziff, *Precise determination of the bond percolation thresholds and finite-size scaling corrections for the sc, fcc, and bcc lattices*, Phys. Rev. E **57**, 230 (1998).
- [34] P. E. Berche, C. Chatelain, B. Berche, and W. Janke, *Bond dilution in the 3D Ising model: A Monte Carlo study*, Eur. Phys. J. B **38**, 463 (2004).
- [35] L. Turban, *Effective-medium approximation for quenched bond-disorder in the Ising model*, Phys. Lett. A **75**, 307 (1980).
- [36] M. E. Fisher and H. Au-Yang, *Inhomogeneous differential approximants for power series*, Journal of Physics A: Mathematical and General **12**, 1677 (1979).
- [37] A. J. Guttmann, *Asymptotic analysis of power-series expansions*, in vol. 13 of *Phase Transitions and Critical Phenomena*, edited by C. Domb and J. L. Lebowitz (Academic Press, New York, 1989), pp. 1–234.
- [38] G. A. Baker and D. L. Hunter, *Methods of series analysis II*, Phys. Rev. B **7**, 3377 (1973).

- [39] L. Klein, J. Adler, A. Aharony, A. B. Harris, and Y. Meir, *Series expansions for the Ising spin glass in general dimension*, Phys. Rev. B **43**, 11249 (1991).
- [40] P. Calabrese, V. Martín-Mayor, A. Pelissetto, and E. Vicari, *Three-dimensional randomly dilute Ising model: Monte Carlo results*, Phys. Rev. E **68**, 036136 (2003).
- [41] H. G. Ballesteros, L. A. Fernández, V. Martín-Mayor, A. Muñoz Sudupe, G. Parisi, and J. J. Ruiz-Lorenzo, *Critical exponents of the three-dimensional diluted Ising model*, Phys. Rev. B **58**, 2740 (1998).
- [42] R. Folk, Y. Holovatch, and T. Yavors'kii, *Effective and asymptotic critical exponents of weakly diluted quenched Ising model: 3d approach versus  $\sqrt{\epsilon}$ -expansion*, Phys. Rev. B **61**, 15114 (2000).
- [43] D. P. Belanger, A. R. King, and V. Jaccarino, *Crossover from random-exchange to random-field critical behavior in  $Fe_xZn_{1-x}F_2$* , Phys. Rev. B **34**, 452 (1986).
- [44] B. Berche, P.-E. Berche, C. Chatelain, and W. Janke, *Random Ising model in three dimensions: theory, experiment and simulation – a difficult coexistence*, Condens. Matter Phys. **8**, 47 (2005).
- [45] S. A. Newlove, *Critical amplitudes for the random Ising system*, J. Phys. C: Solid State Phys. **16**, L423 (1983).
- [46] R. Folk, Yu. Holovatch, and T. Yavors'kii, *Five-loop critical exponents of the weakly diluted Ising model: 3D approach versus square root epsilon-expansion*, J. Phys. Stud. **2**, 213 (1998).
- [47] H. G. Ballesteros, L. A. Fernández, V. Martín-Mayor, A. Muñoz-Sudupe, G. Parisi, and J. J. Ruiz-Lorenzo, *Critical behavior in the site-diluted three-dimensional three-state Potts model*, Phys. Rev. B **61**, 3215 (2000).
- [48] D. Ivaneyko, J. Ilnytskyi, B. Berche, and Yu. Holovatch, *Criticality of the random-site Ising model: Metropolis, Swendsen-Wang and Wolff Monte Carlo algorithms*, Condens. Matter Phys. **8**, 149 (2005).
- [49] M. Hellmund and W. Janke, *Star-graph expansions for bond diluted Potts models*, Phys. Rev. E **67**, 026118 (2003).
- [50] C. Chatelain, B. Berche, W. Janke, and P. E. Berche, *Softening of first-order transition in three-dimensions by quenched disorder*, Phys. Rev. E **64**, 036120 (2001).
- [51] C. Chatelain, B. Berche, W. Janke, and P. E. Berche, *Monte Carlo study of phase transitions in the bond-diluted 3D 4-state Potts model*, Nucl. Phys. B **719** [FS], 275 (2005).
- [52] W. Janke and S. Kappler, *Multibondic cluster algorithm for Monte Carlo simulations of first-order phase transitions*, Phys. Rev. Lett. **74**, 212 (1995).
- [53] M. S. Carroll, W. Janke, and S. Kappler, *Dynamical behavior of the multibondic and multicanonic algorithm in the 3D q-state Potts model*, J. Stat. Phys. **90**, 1277 (1998).
- [54] J. T. Chayes, L. Chayes, D. S. Fisher, and T. Spencer, *Finite-size scaling and correlation lengths for disordered systems*, Phys. Rev. Lett. **57**, 2999 (1986).
- [55] M. Hellmund and W. Janke, *Random-bond Potts models on hypercubic lattices: High-temperature series expansions*, Nucl. Phys. B (Proc. Suppl.) **106–107**, 923 (2002).
- [56] M. Barma and M. E. Fisher, *Two-dimensional Ising-like systems: Corrections to scaling in the Klauder and double-Gaussian models*, Phys. Rev. B **31**, 5954 (1985).